



Effect of Unidirectional and Cross-Rolling on the Texture Evolution of a Hot Extruded AA6082 [†]

Majid Yazdani ^{1,*} , Clément Pot ¹, Quentin Boyadjian ¹, Yang Liu ², Stephen Yue ², Jean-François Béland ³ and Philippe Bocher ¹ 

¹ Département de Génie Mécanique, École de Technologie Supérieure, 1100 Rue Notre-Dame Ouest, Montréal, QC H3C 1K3, Canada; clement.pot.2@ens.etsmtl.ca (C.P.); quentin.boyadjian.1@ens.etsmtl.ca (Q.B.); philippe.bocher@etsmtl.ca (P.B.)

² Materials Engineering Department, McGill University, Wong Building, 3610 University, Montréal, QC H3A 0C5, Canada; yang.liu9@mail.mcgill.ca (Y.L.); steve.yue@mcgill.ca (S.Y.)

³ Conseil National de Recherches Canada, 501 Boulevard de l'Université Est, Saguenay, QC G7H 8C3, Canada; jean-francois.beland@cnrc-nrc.gc.ca

* Correspondence: majid.yazdanieismaeilabad.1@ens.etsmtl.ca

[†] Presented at the 15th International Aluminium Conference, Québec, QC, Canada, 11–13 October 2023.

Abstract: To illustrate how the texture evolution of a polycrystalline aluminum alloy is dependent on the deformation path, hot extruded AA6082 plates in T6 conditions were rolled with various deformation modes. Unidirectional and cross-rolling were conducted at room temperature for different levels of thickness reduction. The resulting textures were then evaluated using the electron backscatter diffraction technique. Depending on the extent of deformation, different textures were obtained. The strong texture of the initial hot extruded material influences texture development and provides new insights into texture development in aluminum alloys. The evolution of the Cube component was particularly interesting in this matter. A competition between dislocation glide and crystal rotation could explain the observed results. The comprehension of these mechanisms leads to a better understanding of texture evolution that drives many properties in aluminum alloys.

Keywords: cold rolling; unidirectional rolling; cross-rolling; texture analysis; EBSD measurement; AA6082



Citation: Yazdani, M.; Pot, C.; Boyadjian, Q.; Liu, Y.; Yue, S.; Béland, J.-F.; Bocher, P. Effect of Unidirectional and Cross-Rolling on the Texture Evolution of a Hot Extruded AA6082. *Eng. Proc.* **2023**, *43*, 28. <https://doi.org/10.3390/engproc2023043028>

Academic Editor: Houshang Alamdari

Published: 18 September 2023



Copyright: © 2023 by the authors. Licensee MDPI, Basel, Switzerland. This article is an open access article distributed under the terms and conditions of the Creative Commons Attribution (CC BY) license (<https://creativecommons.org/licenses/by/4.0/>).

1. Introduction

Aluminum alloys are the second most widely used metallic structural materials and are used in the broadest range of products [1]. Their face-centred cubic (FCC) atomic structure and their high stacking fault energy (SFE) exhibit a distinctive crystallographic texture evolution during various stages of material processing [2]. Crystallographic texture, which expresses the statistical distribution of grain orientations, plays a central role in the performance of metals and alloys. Deformed and recrystallized aluminum alloys exhibit distinct crystallographic textures that can generate different level of mechanical anisotropy depending on the deformation level and recrystallization percentage [3,4]. One of the deformation processes that is used to control deformation textures is the rolling process [5].

Rolling is a deformation process that involves applying compressive forces using opposing rolls to decrease the thickness of a sample while keeping its width almost constant (plane strain conditions) [6]. The reduction in thickness during cold rolling increases the mechanical strength of the processed alloys. The higher the reduction, the higher the dislocation density within the material, thereby increasing the stored energy that subsequently triggers recrystallization during heat treatment [5,7]. Previous studies [5,8,9] have reported that Copper ($\{112\} \langle 111 \rangle$), Brass ($\{110\} \langle 112 \rangle$), and S ($\{123\} \langle 634 \rangle$) orientations are prominent components of the plane strain rolling texture observed in polycrystalline aluminum. The deformation textures become stronger as the grains get elongated in the rolling direction during deformation. Several factors, including the deformation path, rolling

geometry, friction, deformation temperature, initial grain size, shear banding, presence of second-phase particles, and rolling reduction, impact the development of deformation texture [5,8,9].

Several research studies offer significant contributions to the understanding of processing parameters on the microstructure and texture properties of aluminum alloys. Kumar et al. [7] focused on the microstructure and texture evolution of AA3003 alloy during different deformation processes, observing that the microstructure exhibited elongated grains and a banded structure along the rolling direction as a result of cold rolling. Cold rolling led to the formation of strong Brass, Copper, and S components while the Cube orientation decreased. Studying the evolution of AA2195 alloy during T6 heat treatment for samples process using different deformation paths, namely cross-rolling (CR) and unidirectional rolling (UDR), Nayan et al. [8] found that the CR sample exhibited an initial Brass texture, which later weakened after thermal treatment, whereas the UDR sample showed an initial Copper texture that transformed into a Cube component after thermal treatment. Chrominski and Lewandowska [10] conducted a study on the texture evolution of AA6082 alloy in the CR condition for the as-extruded sample. The initial fibrous texture transformed into a random texture after a 50% reduction. Furthermore, with further reductions to 70%, the texture evolution exhibited a different pattern, with a notable increase in the intensity of the Brass component.

Despite numerous studies investigating the microstructure and texture evolution of aluminum alloys under various deformation processes, there is a scarcity of information concerning texture evolution under different deformation paths or rolling modes, particularly for initial states in which the microstructure/texture has been stabilized by another deformation process (here extrusion). Therefore, the present work reports the variations of texture for different cold rolling reductions in UDR and CR of a hot extruded AA6082.

2. Materials and Methods

In this investigation, AA6082 in the T6 condition was used. It is an aluminum-magnesium-silicon (Al-Mg-Si) alloy with composition details in Table 1. The material was provided as an extruded rod with a diameter of 58 mm.

Table 1. Chemical composition of the tested alloys.

Alloy	Mg	Si	Cu	Mn	Cr	Fe	Al
AA6082	0.64	0.85	0.01	0.39	0.13	0.16	Bal.

UDR and CR tests were performed to investigate the effects of thickness reductions on the samples. The tests involved multiple passes with the average reduction being 2.5% per pass, resulting in thickness reductions of 20% and 60%. The initial sample dimensions for UDR and CR experiments were $50 \times 70 \times 5$ mm and $50 \times 40 \times 5$ mm, respectively. Cold rolling in the extrusion direction (ED) has a minimal effect on the texture because the microstructure is already stable for elongation in this direction; the UDR tests were performed perpendicular to the extrusion direction. This research outlines how the crystallographic texture generated during extrusion gets destabilized by cold deformation in the opposite direction. In CR, the samples underwent a 90° rotation around the normal direction (ND) between each 2.5% rolling pass. This rotation causes the transverse direction (TD) of the previous rolling pass to become the new rolling direction (RD) for the current pass. For the CR samples, the initial direction of the test was the same as that of the UDR (perpendicular to the ED).

For examining texture and microstructure evolution under electron backscatter diffraction (EBSD) analysis, samples were cut from the center of the deformed metal and cold-mounted. Figure 1 illustrates the step-by-step process of acquiring orientation maps through the EBSD test. The metallographic samples were cold-mounted using resin epoxy and then ground using silicon carbide grinding paper with varying grades (240/480/600/800/1200) to achieve a smooth surface. Ultrasound cleaners were employed to remove

any debris remaining on the sample surfaces after grinding. The samples were further polished using diamond particle solutions with particle sizes of 9, 3, and 1 μm . In order to obtain an optimal surface quality for EBSD characterization and enhance the indexation, vibrational polishing was conducted for 3 h using 0.05 μm diamond particle solutions. The prepared specimens were subjected to EBSD testing using a Hitachi SU-70 field emission gun scanning electron microscope. The analysis focused on the central area of the specimen, with the RD positioned perpendicular to the surface, i.e., the EBSD testing was performed on sections along the ND and TD. The ATEX software [11] was used to analyze the EBSD data and generate various representations such as the EBSD map, Pole Figure (PF), and the Inverse Pole Figure (IPF). Figure 1 also displays the color code and the designated TD-ND section used for all EBSD maps.

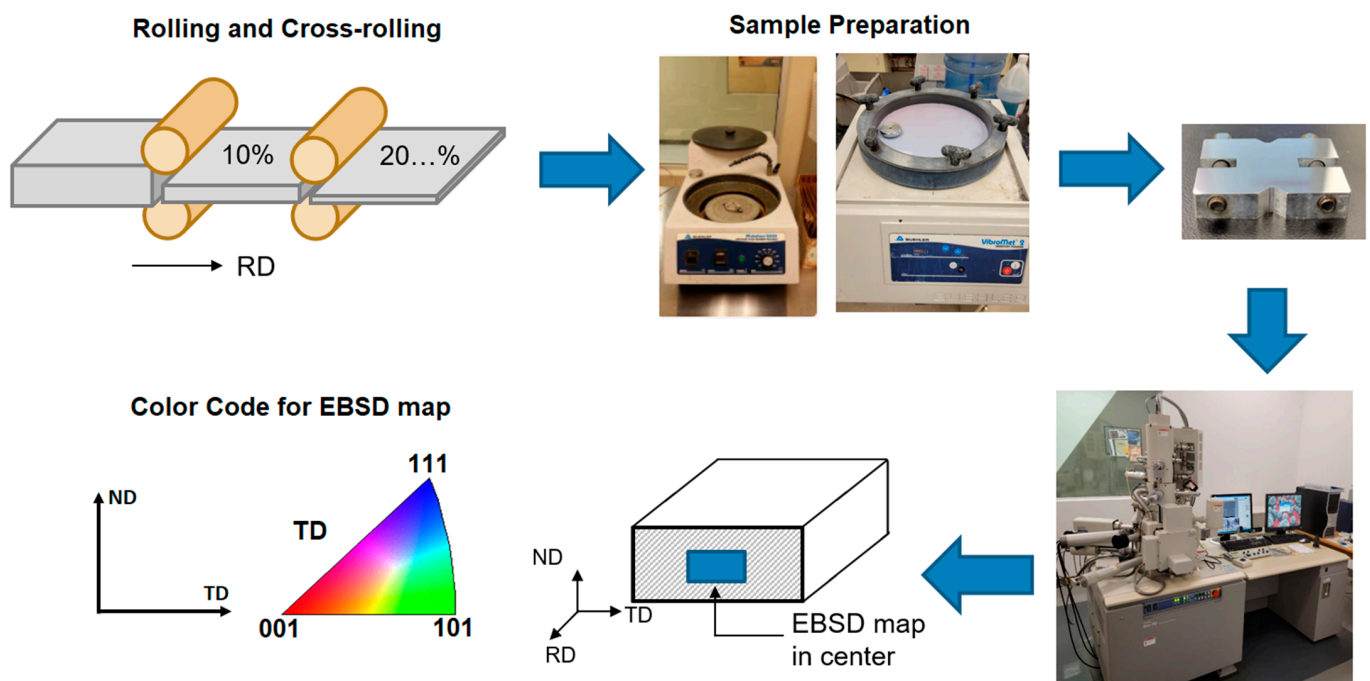


Figure 1. Illustration of the process to acquire the results from the EBSD analysis.

3. Results

The as-received sample has a fibrous structure and exhibited a double fiber texture, where the $\langle 001 \rangle$ and $\langle 111 \rangle$ orientations aligned parallel to the extrusion direction (TD) since the rolling direction is transverse to the extrusion direction), as illustrated in Figure 2 displaying the IPF and EBSD map of the as-received sample. The $\langle 001 \rangle$ fiber is represented by the red color, while the $\langle 111 \rangle$ fiber is depicted in blue. Figure 2 also provides IPFs of the as-received sample. The IPFs confirm the findings obtained from the EBSD map. The analysis reveals the presence of a two-fibrous texture, namely $[111] \parallel \text{TD}$ and $[001] \parallel \text{TD}$, with intensities of 13.66 and 5.5 multiples of random distribution (mrd) or $\times R$, respectively. This indicates that the $[111]$ and $[001]$ crystallographic directions of many grains align parallel to the transverse direction of the initial sample. Furthermore, a relatively weaker orientation in $[101] \parallel \text{RD}$ with an intensity of $2.92 \times R$ is observed before rolling the samples.

In the UDR condition, upon rolling with a 20% reduction, there were no significant changes observed in the microstructure, and the double fiber texture remained intact, as depicted in Figure 3a. However, with a further increase in reduction up to 60%, the thickness of the layers decreased, leading to the appearance of new color variations, indicating deviations from the initial orientation (see Figure 3b). In certain regions, the red color representing the $\langle 001 \rangle$ fiber faded, and new orientations increased. The IPFs also reveal a decrease in the intensities of $[111] \parallel \text{TD}$ and $[001] \parallel \text{TD}$ orientations with increasing rolling reductions, reaching values of $6.4 \times R$ and $2.21 \times R$ at a 60% reduction, respectively. Addi-

tionally, it is evident that a new orientation emerged in the rolling direction ($[111] \parallel \text{RD}$) with increasing reductions $[101] \parallel \text{RD}$ orientations diminished as rolling is conducted in the transverse direction.

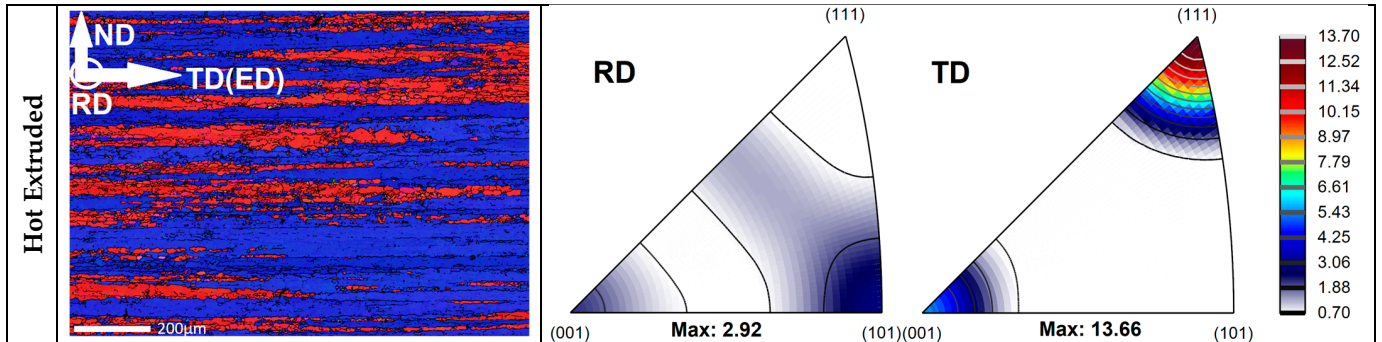


Figure 2. EBSD map and IPF for the as-received material (hot extruded).

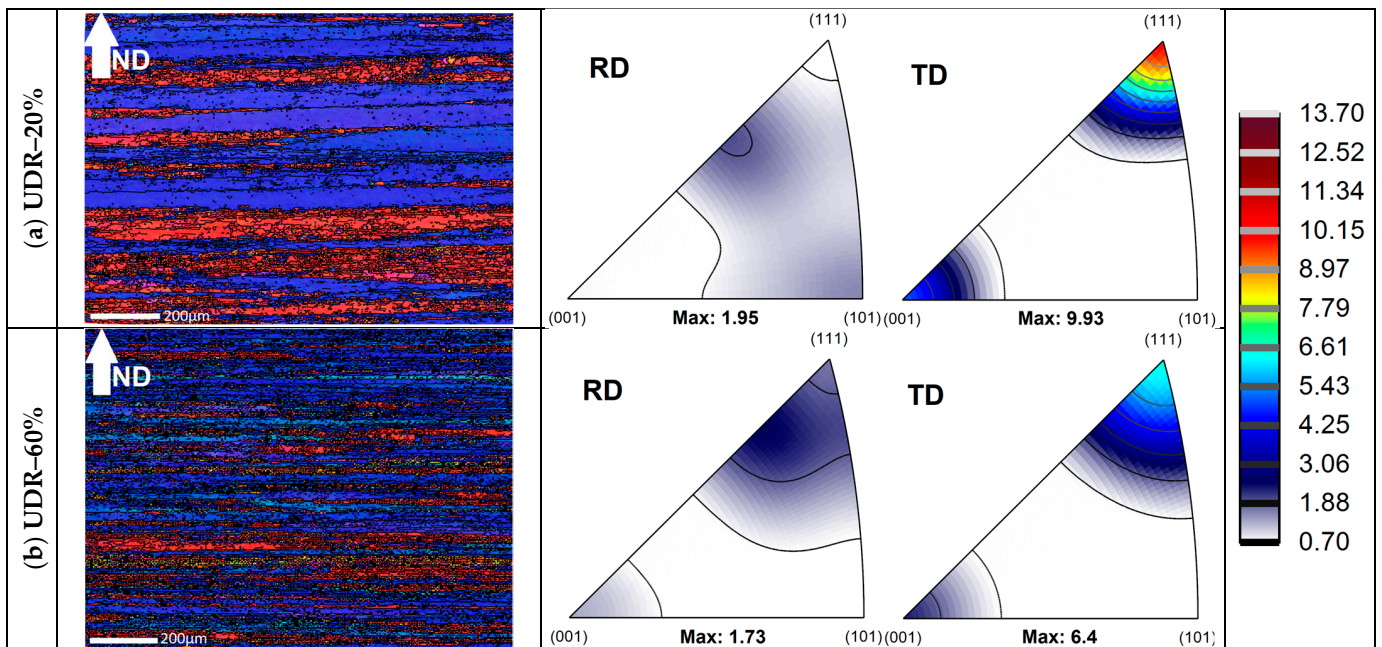


Figure 3. EBSD map and IPF of UDR sample; (a) after 20% reduction, and (b) after 60% reduction.

In Figure 4, the changes in texture during cross-rolling of the as-received materials are depicted using EBSD maps and IPF representations. In the EBSD maps, the colors used to represent orientations in these images are aligned with TD (Figure 1) to track changes in the initial fibers. As previously mentioned, the as-received material exhibits two distinct fibers, and their orientations remain relatively unchanged, with a 20% reduction. After a 60% reduction (Figure 4b), the initial fiber axes can still be observed, although the $\langle 111 \rangle$ fiber is relatively weakened compared to the as-received material. Figure 4 also displays the IPFs of cross-rolled samples. As the rolling reductions increase to 60%, the previously strong orientations of $[111] \parallel \text{TD}$ and $[001] \parallel \text{TD}$ show a weakening trend, resulting in decreased intensities to the value of $5.34 \times R$ and $4.73 \times R$, respectively. In contrast, a new texture component, $[111] \parallel \text{RD}$, emerges with an intensity of $2.15 \times R$. Additionally, like the UDR condition, the existing texture components of $[101] \parallel \text{RD}$ are eliminated.

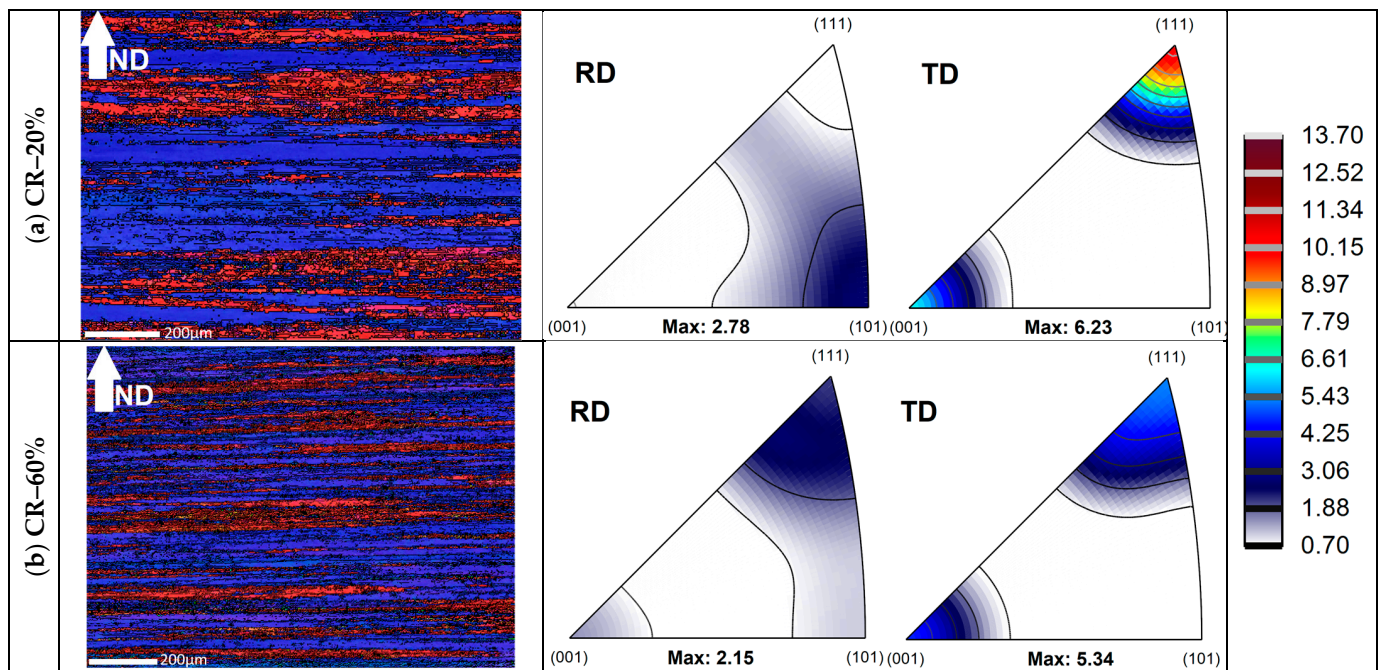


Figure 4. EBSD map and IPF of CR sample: (a) after 20% reduction, and (b) after 60% reduction.

The results clearly indicate a significant change in texture evolution with increasing reductions, as illustrated by the (111) PFs in Figure 5. The transition from an initially axially symmetric texture (Figure 5a) towards the Brass component becomes more evident in the sample rolled with a 60% reduction for both conditions (Figure 5c,e). Table 2 presents the texture components in different conditions, providing a clearer understanding of the texture variation with increasing reductions. The analysis reveals that the Cube component exhibits a maximum value in the as-received material. However, as the reductions increase to 20%, the Cube component decreases, but it subsequently increases with further reductions in both conditions at 60%. Alongside the Cube component, the Brass and S components remain substantial in all conditions. On the other hand, the Goss and Copper components exhibit negligible amounts across all conditions.

Table 2. Texture components in different conditions.

Component, Symbol	{hkl}<uvw>	Conditions				
		As-Received	UDR20	UDR60	CR20	CR60
Cube	{001} < 100 >	17.45	5.25	10.58	7.25	10.17
Goss	{011} < 100 >	0.04	0.04	1.31	0.046	0.2
Brass	{011} < 211 ⁻ >	56.02	63.92	63.38	62.89	69.09
S	{123} < 634 ⁻ >	26.42	30.69	23.18	29.69	20.23
Copper	{112} < 11 ⁻ 1 ⁻ >	0.006	0.029	0.8	0.044	0.05
	Other	0.064	0.071	0.75	0.08	0.26

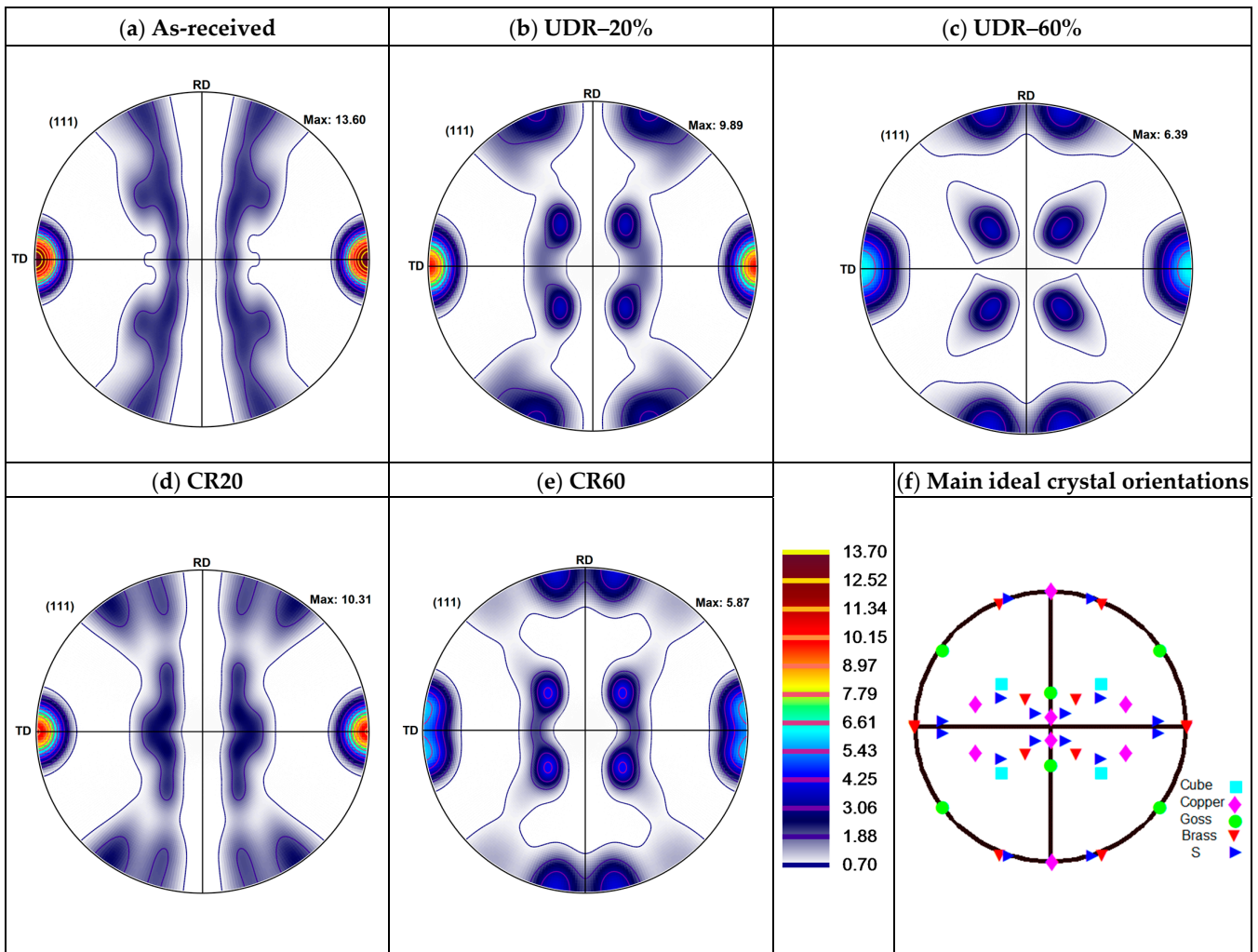


Figure 5. PFs in different conditions: (a) As-received condition, (b) UDR after 20% reduction, (c) UDR after 60% reduction, (d) CR after 20% reduction, and (e) CR after 60%, and (f) Main ideal crystal orientation.

4. Discussions

The as-received material, which corresponds to the hot extruded sample, exhibits a fibrous structure that can be attributed to the characteristic nature of AA6082. This alloy is well-known for its fibrous structure following the extrusion process. This fibrous structure is believed to be formed by the presence of numerous dispersoids in the alloy, which effectively hinder the process of recrystallization during the extrusion process [12].

In addition, the initial material demonstrates a distinctive double fiber texture, with the $\langle 001 \rangle$ and $\langle 111 \rangle$ orientations aligned parallel to the extrusion direction (Figure 2). This characteristic fiber texture is commonly observed in non-recrystallized aluminum alloy extruded profiles, as documented by various researchers [10,13]. In addition, the initial orientations of the as-received material include the presence of Brass and S components, which are part of the β -fiber. The β -fiber, consisting of the Brass, S, and Copper components, is commonly observed in the deformation texture of FCC materials [13]. The as-received material displays a strong Cube component in its texture, which is attributed to the influence of plane strain compression. Additionally, the deformation process gave rise to heterogeneities that contribute to the formation of Cube-oriented grains in FCC materials [14].

In the case of UDR, early stages of deformation result in dislocation activities that induce grain rotation toward efficient slip activity. These combined mechanisms generate the

expected texture components, particularly the dominant Brass and S orientations (Figure 5 and Table 2). Our findings align with previous studies conducted by Nayan et al. [8] and Bhattacharjee et al. [15], which reported the presence of Brass and S orientations in the rolled samples. However, in contrast to their findings, the amount of Copper orientation in this study is negligible. Furthermore, even after undergoing a 60% reduction, the material retained its fibrous structure along the extrusion direction. This can be attributed to the fact that the initial material had a strong initial texture from the as-received state, which made it resistant to significant changes even after substantial reductions. The reduced presence of Cube components after a 20% reduction indicates that grain rotations have a more pronounced effect under this condition. As the reduction is increased up to 60%, the thickness of the regions belonging to the same fiber is reduced. The $\langle 001 \rangle$ fiber fades and leads to the emergence of new orientation, i.e., color variations in the IPFs (Figure 3b). In certain regions, the red color representing and gives way to new orientations, indicated by the violet and yellow colors along TD. Furthermore, there is a notable decrease in the amount of the Cube component at a 20% reduction, followed by an increase at higher reduction levels (60%), although it remains lower than that of the as-received material. This finding contradicts some previous studies, which reported a decrease in the amount of Cube orientation with increasing rolling reduction. According to these studies, the Cube component is considered metastable and undergoes conversion into the β fiber component during cold rolling [16]. Previous studies have also observed that at rolling reductions up to 63%, the initial Cube orientation is retained but exhibits a significant scatter in orientation [17]. In this study, the distinct behavior can be attributed to the strong initial texture, which exhibits different characteristics compared to conventional behavior, necessitating further analysis.

In the CR condition, it was observed that the changes in texture evolution align with the changes observed in the UDR condition but with different kinetics. Previous studies [8,10,18] have reported that a change in the deformation path during the deformation process impacts the plastic behavior of metals, leading to the destabilization of the dislocation substructure after each pass. In this study, it was observed that changing the deformation path maintained the characteristics of the initial texture. The Brass component increased in CR60 (69.09%) compared to the UDR condition (63.38%) as shown in Table 2. Conversely, the S and Copper components exhibited a decrease from 23.18% and 0.8% in UDR60 to 20.23% and 0.05% in CR60, respectively. These variations can be attributed to the inherent nature of the CR process. The multiple changes in the rolling direction during each pass activate different slip systems and induce multidirectional rotations, ultimately altering the texture behavior of the processed material. In our investigation, it is worth highlighting that although the Brass component exhibits the highest fraction among the various components, the presence of significant amounts of S and Cube components is also noteworthy. If the decrease in Cube orientation compared to the initial material after a 20% reduction, its reduction in intensity is less significant than for the UDR. With further reduction, the Cube component increases more significantly than the UDR, although it remained lower than the initial amount. Previous studies [8,10,19] examining different materials such as cast and homogenized AA2195 alloy, as-extruded AA6082, and forged and annealed electric copper samples have indicated that the Brass component is the dominant component in the texture after cross-rolling. This could be attributed to the fact that the previous studies concentrated mostly on higher levels of reduction, whereas our reductions were comparatively lower. Therefore, it is conceivable to expect that with increasing the reductions to higher levels in our research, the texture evolution will likely exhibit a stronger alignment with the Brass component and become more pronounced.

5. Conclusions

This study investigated the texture evolution of as-received AA6082 under different modes of cold rolling. The as-received material exhibited a fibrous structure, attributed to the presence of dispersoids that impede recrystallization during extrusion. The texture

evolution in both the cross-rolling (CR) and unidirectional rolling (UDR) conditions showed similar changes, albeit with different kinetics. Despite undergoing a significant 60% reduction, the materials retained their fibrous structure along the extrusion direction due to the strong initial texture. The deformation processes induced dislocation activities and grain rotations, resulting in the dominant Brass and S orientations. The texture behavior was influenced by the CR process, leading to an increase in the Brass component and a decrease in the S and Copper components compared to UDR. Additionally, the Cube orientation exhibited a lesser reduction in intensity during CR, indicating its greater stability under this condition.

Author Contributions: Conceptualization, C.P., M.Y., Q.B., P.B., Y.L. and S.Y.; methodology, C.P., M.Y., Q.B., J.-F.B., P.B., Y.L. and S.Y.; writing—review and editing, C.P., Q.B., M.Y. and P.B.; supervision, P.B.; funding acquisition, P.B. All authors have read and agreed to the published version of the manuscript.

Funding: The APC was funded by the National Research Council and Natural Sciences and Engineering Research Council Canada.

Institutional Review Board Statement: Not applicable.

Informed Consent Statement: Not applicable.

Data Availability Statement: No new data were created or analyzed in this study. Data sharing is not applicable to this article.

Acknowledgments: The authors are grateful to NRC Canada and Rio Tinto for their technical support.

Conflicts of Interest: The authors declare no conflict of interest.

References

1. Sheppard, T. *Extrusion of Aluminium Alloys*; Springer: New York, NY, USA, 1999. Available online: <https://books.google.com/books?id=8bm1gbGAGbAC> (accessed on 10 July 2023).
2. Hirsch, J. Texture evolution during rolling of aluminum alloys. In *Light Metals-Warrendale-Proceedings*; TMS: Pittsburgh, PA, USA, 2008; p. 1071.
3. Thomsen, S.; Hopperstad, O.S.; Børvik, T. Anisotropic Plasticity and Fracture of Three 6000-Series Aluminum Alloys. *Metals* **2021**, *11*, 557. [[CrossRef](#)]
4. Fukutomi, H.; Okayasu, K. Control of Textures in Aluminum Solid Solution Alloys by High-Temperature Deformation. In *Proceedings of the 8th Pacific Rim International Congress on Advanced Materials and Processing*; Marquis, F., Ed.; Springer International Publishing: Cham, Switzerland, 2013; pp. 965–972.
5. Humphreys, F.J.; Hatherly, M. (Eds.) Chapter 3-Deformation Textures. In *Recrystallization and Related Annealing Phenomena*, 2nd ed.; Elsevier: Oxford, UK, 2004; pp. 67–89. [[CrossRef](#)]
6. Groover, M.P. *Fundamentals of Modern Manufacturing: Materials, Processes, and Systems*; John Wiley & Sons: Hoboken, NJ, USA, 2020.
7. Kumar, R.; Gupta, A.; Dandekar, T.R.; Khatirkar, R.K. Microstructure and texture development in AA3003 aluminium alloy. *Mater. Today Commun.* **2020**, *24*, 100965. [[CrossRef](#)]
8. NNayan; Mishra, S.; Prakash, A.; Murty, S.V.S.N.; Prasad, M.J.N.V.; Samajdar, I. Effect of cross-rolling on microstructure and texture evolution and tensile behavior of aluminium-copper-lithium (AA2195) alloy. *Mater. Sci. Eng. A* **2019**, *740–741*, 252–261. [[CrossRef](#)]
9. Lee, D.N. Relationship between deformation and recrystallisation textures of fcc and bcc metals. *Philos. Mag.* **2005**, *85*, 297–322. [[CrossRef](#)]
10. Chrominski, W.; Lewandowska, M. Effect of Fiber Orientation on Microstructure and Texture Evolution During the Cold-Rolling of Al–Mg–Si Alloy. *Adv. Eng. Mater.* **2022**, *24*, 2101610. [[CrossRef](#)]
11. Beausir, B.; Fundenberger, J.-J. *Analysis Tools for Electron and X-ray Diffraction, ATEX-Software*; Université de Lorraine: Metz, France, 2017.
12. Rakhmonov, J.; Liu, K.; Rometsch, P.; Parson, N.; Chen, X.-G. Effects of Al(MnFe)Si dispersoids with different sizes and number densities on microstructure and ambient/elevated-temperature mechanical properties of extruded Al–Mg–Si AA6082 alloys with varying Mn content. *J. Alloys Compd.* **2021**, *861*, 157937. [[CrossRef](#)]
13. Zhang, C.; Wang, C.; Zhang, Q.; Zhao, G.; Chen, L. Influence of extrusion parameters on microstructure, texture, and second-phase particles in an Al–Mg–Si alloy. *J. Mater. Process. Technol.* **2019**, *270*, 323–334. [[CrossRef](#)]
14. Dons, A.L.; Nes, E. Nucleation of cube texture in aluminium. *Mater. Sci. Technol.* **1986**, *2*, 8–18. [[CrossRef](#)]
15. Bhattacharjee, P.P.; Joshi, M.; Chaudhary, V.P.; Zaid, M. The effect of starting grain size on the evolution of microstructure and texture in nickel during processing by cross-rolling. *Mater. Charact.* **2013**, *76*, 21–27. [[CrossRef](#)]

16. Liu, W.C.; Man, C.-S.; Morris, J.G. Lattice rotation of the cube orientation to the β fiber during cold rolling of AA 5052 aluminum alloy. *Scr. Mater.* **2001**, *45*, 807–814. [[CrossRef](#)]
17. Engler, O.; Kong, X.W.; Lücke, K. Development of microstructure and texture during rolling of single-phase and two-phase cube-oriented Al-Cu single crystals. *Scr. Mater.* **1999**, *41*, 493–503. [[CrossRef](#)]
18. Zhang, Z.; Chen, D.; Zhao, H.; Liu, S. A comparative study of clock rolling and unidirectional rolling on deformation/recrystallization microstructure and texture of high purity tantalum plates. *Int. J. Refract. Met. Hard Mater.* **2013**, *41*, 453–460. [[CrossRef](#)]
19. Hong, S.-H.; Lee, D.N. Deformation and Recrystallization Textures in Cross-Rolled Copper Sheet. *J. Eng. Mater. Technol.* **2001**, *124*, 13–22. [[CrossRef](#)]

Disclaimer/Publisher's Note: The statements, opinions and data contained in all publications are solely those of the individual author(s) and contributor(s) and not of MDPI and/or the editor(s). MDPI and/or the editor(s) disclaim responsibility for any injury to people or property resulting from any ideas, methods, instructions or products referred to in the content.